Supramolecular Properties of the Proline-Rich γ-Zein N-Terminal Domain

Marcelo J. Kogan,* Ionara Dalcol,* Pau Gorostiza,† Carmen Lopez-Iglesias,‡ Ramon Pons,§ Miquel Pons,* Fausto Sanz,† and Ernest Giralt*

*Departament de Química Orgànica, †Departament de Química Física, and ‡Serveis Científicotècnics, Parc Científic de Barcelona, Universitat de Barcelona, 08028-Barcelona, and §Departament de Tensioactius, IIQAB, CID, CSIC, 08034-Barcelona, Spain

ABSTRACT Zeins are maize storages proteins that accumulate inside large vesicles called protein bodies. γ-Zein lines the inner face of the protein body membrane, and its N-terminal proline-rich repetitive domain with the sequence $(VHLPPP)_8$ appears to be necessary for the accumulation of the protein within the organelle. Synthetic $(VHLPPP)_8$ adopts an amphipathic polyproline II conformation. In a preliminary recent work we used atomic force microscopy to study the surface organization of the octamer and transmission electron microscopy to visualize aggregates of the peptide from aqueous solution. We previously envisioned two self-assembly models (i.e., the geometric and the micellar) that take into account the observed features. In the present work we studied in detail the self-assembly of the peptide in solution and found that the peptide is able to form cylindrical micelles. Fibrils formed on graphite are generated by assembly of solution micelles. Based on the results of these studies, we focused exclusively on the micellar model. To our knowledge we have characterized for the first time supramolecular aggregates of polyproline structures other than collagen. The spontaneous arrangement of $(VHLPPP)_8$ suggests a role for the N-terminal domain of γ-zein in the process of the whole protein deposition in protein bodies.

INTRODUCTION

Amphipathic secondary structures play an important role in protein folding, in protein-protein interactions, and in the self-assembly of either natural or designed peptides. An amphipathic helix results when the periodicity of a regular pattern of hydrophobic and hydrophilic residues throughout the sequence matches the number of residues per turn. In the well-known amphipathic α-helix, the typical sequence has hydrophobic residues every three or four residues, matching the 3.6 residues per turn of the canonical α-helix. Polyproline in aqueous solution adopts a left-handed helical structure known as polyproline II (PPII). This rather extended helix has three residues per turn, and its structural and functional importance is becoming more apparent (Williamson, 1994). In particular, this conformation is found in a number of proline-rich peptides containing a variety of residues. PPII plays a key role in protein-protein contacts mediated by SH3 (Wu et al., 1995), in WW domains (Staub and Rotin, 1996), and in peptides bound to class II histocompatibility proteins (Stern et al., 1994). Moreover, the PPII helix may well be a critical conformational element in many conformational diseases (Blanch et al., 2000; Gill et al., 2000).

Storage proteins in cereals are especially rich in proline-rich domains (Showalter, 1993). γ-Zein is a major constituent of maize storage proteins and accumulates with α-zeins in endoplasmic reticulum (ER)-derived protein bodies (Ludevid et al., 1984). The nature of the physical interactions between proteins that are responsible for the assembly of protein bodies is fairly well known. Lending (1996) suggested the formation of a tubular array, possibly formed by zeins, associated with protein bodies at 22 days after pollination in the rough ER of opaque-2 maize (an endosperm mutant in which the presence of α-zein is low and γ-zein is high). γ−Zein lines the inner face of the protein body membrane (Ludevid et al., 1984) and has three domains: an N-terminal proline-rich repetitive domain (γ-ZNPRD), a $(PX)_n$ repetitive central domain, and a large cysteine-rich C-terminal domain (Geli et al., 1994). The N-terminal domain contains a highly repetitive sequence $(VHLPPP)_8$, which adopts a long amphipathic PPII helix. It has been suggested that the self-assembly of γ-zein through its proline-rich repetitive sequence $(VHLPPP)_8$ provides the ER retention mechanism for this protein (Geli et al., 1994; Herman and Larkins, 1999). In nature, γ-zein-like proteins have been found with repetitive domains consisting of only two complete hexapeptides and two truncated hexapeptides of five and three residues (Shewry and Tatham, 1990).

Several years ago, our group (Dalcol et al., 1995) succeeded in synthesizing a series of peptides of general formula $(VHLPPP)_r$ ($r = 2–8$) using a solid-phase convergent approach (Lloyd-Williams et al., 1997). Studies using circular dichroism have shown that these peptides adopt a PPII conformation in aqueous solution, which increases with the length of the oligomer (Rabanal et al., 1993; Dalcol et al., 1996).

In a recent work we determined by atomic force microscopy that the peptide $(VHLPPP)_8$, which adopts an amphipathic PPII helix conformation (Fig. 1), self assembles forming parallel fibrils over the highly oriented pyrolytic graphite surface (Kogan et al., 2001). In order to relate the

Submitted November 7, 2002, and accepted for publication April 9, 2002.

I. Dalcol's present address: Universidade Federal de Santa Maria, Departamento de Química, Campus Universitario-CAMOBI, Santa Maria-RS, Brasil.

Address reprint requests to Dr. Ernest Giralt, Departament de Química Orgànica, Universitat de Barcelona, Martí i Franquès 1, Barcelona 08028, Spain. Tel.: 34-93-4021249; Fax: 34-93-3397878; E-mail: egiralt@qo.ub.es.

0006-3495/02/08/1194/11 $2.00

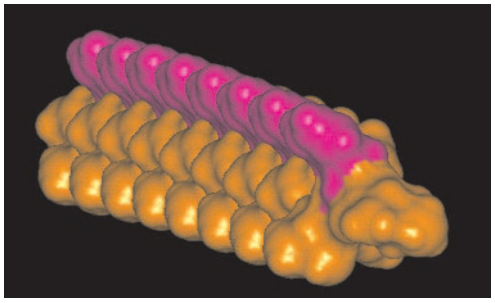

FIGURE 1 Accessible surface of a single octamer molecule modeled adopting a PPII conformation using the Conolly algorithm (implemented in Insight II v.98). The hydrophobic residues (leucine and valine) and neutral residues (proline) are represented in orange, and polar protonated histidine residues are in purple.

fibril's width with the dimensions of the molecule $(VHLPPP)_8$ we proposed two self-assembly models (the geometric model and the micellar one). In the geometric model the formation of the fibrils is determined by the para1lel alignment over the highly oriented pyrolytic graphite surface, where the width of the fibril is related to the length of the molecule. In contrast, in the micellar model the lateral interaction of peptide molecules leads to the formation of cylindrical micelles that deposit over the highly oriented pyrolytic graphite surface giving fibrils in which the PPII helix molecules are aligned in the direction of the fibril axes. Thus, the fibril width is independent of the length of the molecule.

In the present work new experimental results in solution and also on the highly oriented pyrolytic graphite/water interface are described. In-depth analyses of the self-assembly processes both in solution and over the highly oriented pyrolytic graphite/water interface of the peptide $(VHLPPP)_8$ were carried out. Structural characteristics of the peptide in solution were determined by spectroscopy (circular dichroism), scattering measurements (small-angle x-ray scattering), and nanosensitivity techniques (transmission electron microscopy and atomic force microscopy). A wide discussion of the results leads to an understanding of the complex mechanism of self-assembly of the N-terminal domain of γ-zein either in solution or over the highly oriented pyrolytic graphite/water interface. We are confident that these results will help to obtain a greater understanding of the biological role of the N-terminal domain of γ-zein in the ER membrane.

MATERIALS AND METHODS

Peptide solutions

The solutions for all determinations were prepared by dissolution of the corresponding synthetic peptides in milli-Q water. The peptides $(VHLPPP)_r$ were synthesized in its corresponding *r*-trifluoracetate form, according to Dalcol et al. (1995). The pH of the resulting solutions was 5–5.5.

Surface tension

A Wilhelmy plate apparatus was used consisting of a 1-cm platinum plate suspended by a Kruss electrobalance connected to a Kruss processor tensiometer K-12 chart recorder (Hamburg, Germany), which determines directly the real surface tension values at equilibrium. Solutions were measured in a Pyrex 9-cm-diameter well crystallization dish. The plate and the dish were cleaned with a sulfochromic mixture and then with milli-Q water (γ = 71.8 mN/m). The variation between individual measurements of the sample was 0.1 mN/m. The variation between different samples was in the order of 1 mN/m. The surfactant critical micelle concentrations (CMA and CMC) were determined from the abrupt change in slope of the surface tension values versus log peptide concentration.

Circular dichroism

Circular dichroism spectra were recorded with a Jasco J700 spectropolarimeter (Great Dumnow, UK) at a spectral bandwidth of 1 nm, with a time constant of 4 s (scan speed 10 nm/min) and a step resolution of 0.2 nm. Each spectrum was the result of three accumulations. Spectra were measured at concentrations ranging from 1×10^{-4} to 2.5×10^{-1} mM ($48–120 \times 10^{-1}$ mM per residue) and were measured at 25°C. A blank spectrum of milli-Q water was subtracted from each peptide spectrum. Molar ellipticities at each concentration are expressed by decimol of residue.

Small-angle x-ray scattering

Small-angle x-ray scattering was carried out by using a Kratky camera of small angle (Hecus M-Braun, Graz, Austria) and a Siemens KF 760 (3-kW) generator (Karlsruhe, Germany). The wavelength corresponding to the Cu Ka-line(1.542 Å) was used. The linear detector was PSD-OED 50 M-Braun, and the temperature controller was a Peltier KPR AP PAAR (Graz, Austria) model working at 25 ± 0.1°C. The sample, 2 mM $(VHLPPP)_8$ in water, was inserted in a glass capillary of 1 mm diameter. The small-angle x-ray scattering curves were smoothed by using a routine that fits a polynomial of increasing degree as the channel number increases. This routine assures no change in the slopes and in the peak position and sharpness. The smoothed curves were de-smeared using the procedure of Singh and coworkers (Singh et al., 1993). These scattering curves were put on an absolute scale by using the value of transmittance as obtained with a moving slit device and the standard value of water (1.68 m^{-1}) to obtain the efficiency (Zemb et al., 1987), and water was subtracted as background. The small-angle x-ray scattering curves are shown as a function of the scattering vector modulus, $q = 4.\pi/\lambda.\sin(\theta/2)$ where θ is the scattering angle and λ the wavelength of the radiation. The q range obtained with our setup was from 0.2 to 6 nm^{-1}.

The results have been simulated by producing sets of random points within cylinders, which have been distributed in space with their centers ordered in a hexagonal array and in parallel. The axis of each cylinder has been tilted at random by a maximum angle of 0.1 rad. The distances between all pairs of points were evaluated, and the pair distribution function (PDF) was constructed (Galtter, 1990). Ten configurations were evaluated for each run, and the mean PDF was determined. Fourier transformation of this PDF gives the intensity pattern. For the evaluation of the two electronic density models, the points that constitute the cylinders were distributed accordingly. The number of points per cylinder, size step of the PDF, and size step of the Fourier transform were checked for consistency to give the desired range of the scattering curve. In the results shown we have used 5000 points per cylinder and a resolution in the PDF of 0.01 nm.

Freeze-fixation, freeze-drying electron microscopy

Drops of peptide solutions were deposited over uncoated coverslips. Coverslips were cryofixed by projection against a copper block cooled by liquid nitrogen (−196°C) using a cryoblock (Reicher-Jung, Leica). The frozen samples were stored at −196°C in liquid nitrogen until subsequent use. Samples were freeze-dried at −90°C and coated with platinum and carbon using a freeze-etching unit (model BAF-060, BAL-TEC; Liechtenstein). A rotary shadowing of the exposed surface was made by evaporating 1 nm of platinum at an angle of 6° above the horizontal, followed by 10 nm of carbon evaporated at an angle of 90°. The replica was separated from the coverslip by immersion in concentrated hydrofluoric acid, washed twice in distilled water, and digested with 5% sodium hypochlorite for 5–10 min. Finally, the replicas were washed several times in distilled water, broken into small pieces, and collected on Formvar-coated copper grids for electron microscopy. All electron micrographs were obtained using an electron microscope Hitachi 800 MT operating at 75 kV. Several samples (10) were prepared following the same procedure and the results were reproducible.

Atomic force microscopy air experiments

Samples were prepared by placing a droplet of a solution of the peptide on freshly cleaved, highly oriented pyrolytic graphite (HOPG graphite, Advanced Ceramics, Cleveland, OH). Samples were kept in a desiccator with flushing dry nitrogen for 30 min. Atomic force microscopy imaging was performed in air with a Multimode Nanoscope IIIA (Santa Barbara, CA) instrument operated in tapping mode (1-Hz scan frequency) at low tapping amplitude and at the lowest force set-point to improve resolution and minimize damage to the sample. To attain the highest resolution and least disturbance to the sample, we imaged the layers at the lowest possible oscillation amplitude, 0.1–0.2 V in the photodiode signal (corresponding to approximately a few nanometers RMS after amplitude calibration). For that purpose, the method that we used was to acquire simultaneously the topographic and phase signals and then reduce the oscillating amplitude (both drive and set-point), until a decrease of the topographic signal together with a sharp increase in the phase contrast was observed, possibly related with the trapping or snap-in of the tip due to capillary forces. The amplitude was then increased slightly above this value, to restore normal topography and phase at the highest resolution).

Etched silicon atomic force microscopy probes were used (resonant frequency 200–400 kHz, nominal spring contact 20–100 N/m, manufactured by Nanosensors). Width measurements were performed at randomly selected regions of each image, and the images were acquired at randomly selected regions of the sample outside the dry drop. Several samples (30) were prepared following the same procedure, and the results were reproducible. To avoid digital resolution problems, images of a maximum of 500×500 nm^2 and at least 256×256 pixels were acquired, and these measurements were averaged over at least 10 fibrils inside the domain. Usually, resolution atomic force microscopy is limited by the convolution of the surface features with the tip (5–10 nm of curvature radius), but the periodic character of the fibrils allows the resolution to be improved because the measurements are made in the same plane.

Atomic force microscopy liquid experiments

A drop of the peptide $(VHLPPP)_f$ solution was placed on freshly cleaved substrate. Imaging in liquid was carried out using triangle-shaped Si_3N_4 cantilevers (resonant frequency ~8 Hz, nominal spring constant 0.09 N/m, nominal tip diameter 20 nm, manufactured by Olympus, Tokyo, Japan) in tapping mode. Fresh atomic force microscopy probes were used for each sample. Imaging has also been made in contact mode, and similar results were obtained, but fibril damaging was observed (data not shown). In this case the Si_3N_4 cantilevers were observed to bend slowly, as revealed by the drift of the deflection signal and then were allowed to stabilize for at least 1 h before the measurements. Atomic force microscopy imaging was carried out in a Nanoscope IIIA system with an Extend Multimode head (Digital Instruments). The liquid was held by surface tension in the atomic force microscopy liquid cell, so that the cell could be operated without the rubber O-ring.

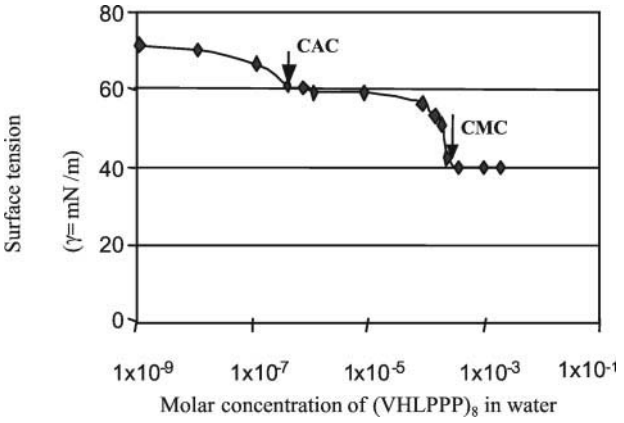

FIGURE 2 Concentration dependence of the effect of $(VHLPPP)_8$ in water surface tension.

Contact angle

One microliter of the peptide $(VHLPPP)_8$ aqueous solution (1×10^{-8} M) or water was deposited on freshly cleaved, highly oriented pyrolytic graphite. The sessile drop (which showed a spherical shape) was observed with a digital video camera (JVC TK-1270). The contact angle was inferred from the measured height (h) and base width or diameter (b) of the drop according to Newman and Good (1979). Several drops (5) were observed following the same procedure.

RESULTS

Surface tension

In a PPII conformation the repetitive sequence VHLPPP will have the hydrophobic residues aligned along one of the faces of the helix while the hydrophilic histidine residues will be aligned in the opposite face (Fig. 1). As we mentioned previously (Kogan et al., 2001), this amphipathic structure acts as a surfactant being able to lower the surface tension of water through the segregation of the amphiphile at the air-water interface directing the hydrophobic moiety away from the aqueous phase. Fig. 2 shows the surface tension measurements of $(VHLPPP)_8$ peptide aqueous solutions for a wide range of concentrations. These results confirm the surfactant properties of the peptide but also reveal a complex behavior with two critical concentrations. Increasing concentrations of $(VHLPPP)_8$ progressively lower the surface tension of water up to a concentration of 4×10^{-7} M. Above this concentration and up to 1×10^{-4} M little additional change in surface tension occurs, defining a critical association concentration (CAC) for the surface action ($\gamma = 62$ mN/m). A sharp fall in γ values can be

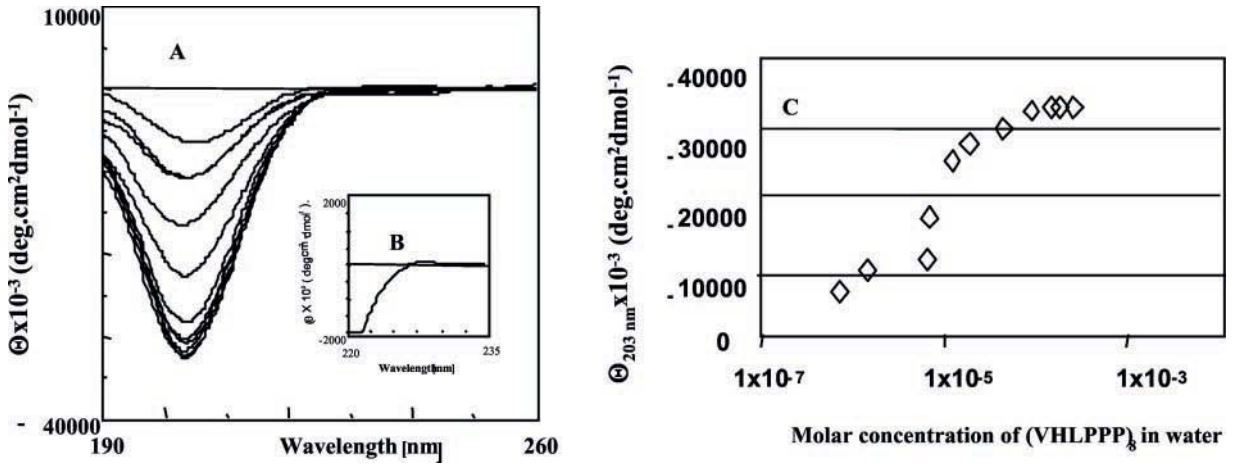

FIGURE 3 (A, B, C). A) Circular dichroism spectra of solution of $(VHLPPP)_8$ in water at different concentrations, B) Circular Dichroism spectra of a 1.4×10^{-4} M aqueous solution of $(VHLPPP)_8$ (amplification in region 220–235 nm). C) Molar ellipticities (θ_{203}) vs. molar concentration of $(VHLPPP)_8$.

seen between 1×10^{-4} and 2×10^{-4} M (from 54 to 42 mN/m, respectively). There is little decrease in surface tension up to concentrations higher than 2×10^{-4} M (considered as the critical micellar concentration, CMC).

Circular dichroism

The circular dichroism spectrum of $(VHLPPP)_8$ in aqueous solution at concentrations above 1.4×10^{-4} M is characteristic of a PPII structure (Fig. 3, *A* and *B*), with an intense negative band centered at 203 nm and a weak positive band at 228 nm (Fig. 3 *B*). This weak band cannot be observed at lower concentrations, but the more intense negative band can be measured at concentrations as low as 2×10^{-7} M. Fig. 3 *A* shows circular dichroism spectra of $(VHLPPP)_8$ as a function of concentration over a range of 2×10^{-7} to 2.5×10^{-4} M. The molar ellipticity of the 203-nm band increases strongly with the peptide concentrations between 4×10^{-7} M (CAC) and 2×10^{-4} M (CMC), the two critical concentrations found in the surface tension measurements (Fig. 3 *C*). Above and below this range of concentrations the molar ellipticity of the 203-nm band is only weakly concentration dependent. However, the $[\theta]$ of the 203-nm band in the high concentration plateau is fourfold higher than in the low concentration part of the curve (Fig. 3 *C*).

Characterization of the aggregates in solution

The presence of two critical concentrations in the surface tension measurements suggests a complex association behavior. At high concentrations, the circular dichroism spectra are concentration independent, and aggregates involve peptide with the maximum PPII content. Between CAC and CMC, peptide aggregation is probably associated with a transition from a disordered to a PPII conformation. Additional information about the aggregates has been obtained in solution by transmission electron microscopy and small-angle x-ray scattering.

Transmission electron microscopy

The peptide solution was freeze-fixed and freeze-dried to preserve the aggregate structures in solution for subsequent transmission electron microscopy imaging after coating the sample with platinum and carbon. The replicas obtained showed the presence of fibrillar superstructures for the octamer (Kogan et al., 2001) of $\sim 20 \pm 2$ nm ($n = 10$) in width and variable length (500–1000 nm). In the inner part of these superstructures was observed the presence of filaments or cylinders of 3 ± 0.7 nm ($n = 10$) in width. To understand the role of the molecule dimension in the registered structures by transmission electron microscopy, we have studied the aggregation of peptides synthesized with a lower number of repeats $(VHLPPP)_r$ ($r = 1, 3$). We observed structures similar in width and length as those observed for $(VHLPPP)_8$ (Fig. 4). In particular, the 3-nm-width inner structures are independent of the length of the peptide. The 10^{-5} M peptide aqueous solution was found to be the optimal concentration for systematic preparations for transmission electron microscopy imaging, but peptide aggregation was observed by transmission electron microscopy for solutions of concentrations between 1×10^{-7} and 2×10^{-3} M.

Small-angle x-ray scattering

Small-angle x-ray scattering is a nondestructive technique that can provide information on size and shape in solution conditions. Fig. 5 shows the small-angle x-ray scattering pattern of a 2×10^{-3} M aqueous solutions of $(VHLPPP)_8$. At low values of the scattering vector modulus (q) the

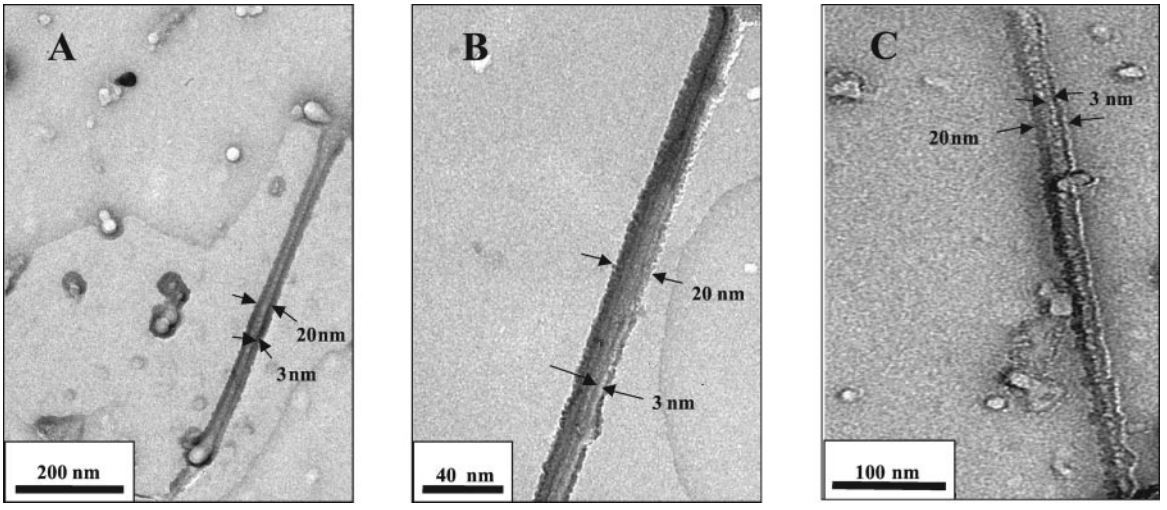

FIGURE 4 Transmission electron microscopy image of the replica obtained after freeze-fixation and freeze-drying of a 2×10^{-5} M aqueous solution of the peptide $(VHLPPP)_r$ over an uncoated coverslip. (*A*) $r = 1$; (*B*) $r = 3$; (*C*) $r = 8$.

intensity sharply increases. A Guinier plot ($\ln I$ versus q^2, data not shown) curves upward, indicating bigger objects as we move to lower q values. In our lower q range we can measure a lower limit for the radius of gyration. The value we obtain for this lower limit is 20 nm. From $q = 0.4$ nm^{-1} to 0.9 nm^{-1} there is a leveling of the scattered intensity and a further decrease at higher q. By using a modified Guinier representation ($\ln Iq$ as a function of q^2, Fig. 5 *A*) a linear region between $q = 1$ nm^{-1} and $q = 4$ nm^{-1} appears, indicative of cylindrical structures. From the slope a diameter for the cylinders of 1.2 nm can be calculated (Porod, 1982). A simulation of the scattering of isolated cylinders (Pedersen, 1997) of 1000 nm length and with a diameter of 1.2 nm (dotted line in Fig. 5 *B*) adequately represents the high q decrease of intensity but clearly does not reproduce the low and medium q features. The leveling at medium q could be produced by interparticle interference (Porod, 1982). On the basis of the transmission electron microscopy results we have simulated this system as a bundle of seven cylinders in a hexagonal arrangement. A simulation assuming particles formed by seven cylinders 1000 nm long and 1.2 nm diameter (Fig. 6), with an interparticle distance of 7 nm, is shown as a dashed line in Fig. 5 *B*. A small degree of angular disorder of the helical axes (<0.1 rad) had to be

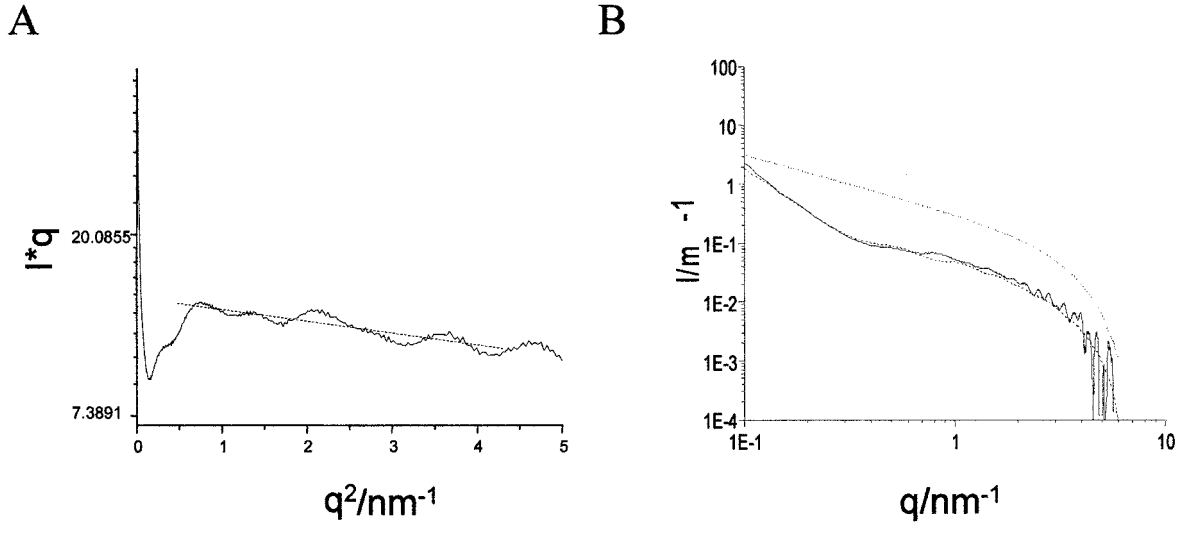

FIGURE 5 (*A*) Modified ($\ln Iq$ vs q^2) Guinier plot. The dashed line corresponds to the linear dependence from which the diameter of cylinders is obtained. (*B*) Scattering intensity versus q (Å^{-1}) for a 2 mM solution of $(VHLPPP)_8$ in water (——). Simulated scattering curve considering a model formed by a cylindrical structure with a length of 1000 nm and a diameter of 1.2 nm (· · ·). Simulated scattering curve considering seven cylinders with an interparticle distance of 7 nm, diameter of 1.2 nm, and 1000 nm length (- - - -).

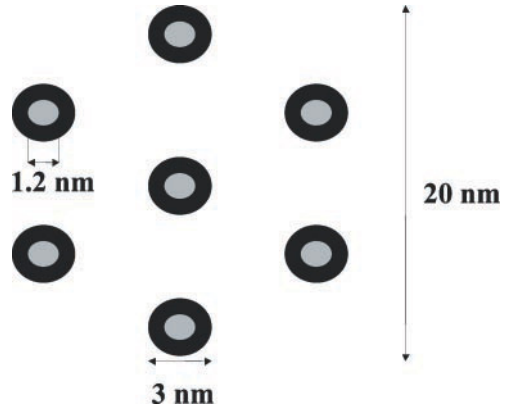

FIGURE 6 Formation of superstructures of the peptide $(VHLPPP)_8$. Frontal view of particles (superstructures) formed by seven cylinders (cylindric micelles) 1000 nm long and 3 nm diameter. A core with a homogeneous electronic density is represented in gray (1.2 nm width was used in the small-angle x-ray scattering simulation). The black parts of the cylinders represent the histidine side chains protruding from the micelle.

introduced in the simulation in a model similar to that used by Schnablegger et al. (1999). All the main features of the scattering curve are adequately represented. Further disordering in the orientation produces the disappearance of the medium q leveling whereas perfect alignment produces a peak in this range. The use of very long cylinders is based on electronic microscopy observations. Agreement between the 1.2-nm diameter obtained by small-angle x-ray scattering and the 3-nm radius observed by transmission electron microscopy can be obtained by assuming that the hydrophobic core is surrounded by a second shell, containing water and the histidine side chains, with a relative contrast lower than 0.04 (either positive or negative) with respect to the surrounding solvent. The cylinder diameter of 1.2 nm (Fig. 6, gray part of the cylinders) is in agreement with the profile of electronic density obtained from the alignment of two octamer molecules aligned in its PPII conformation previously minimized (data not shown, semiempirical calculation carried out with AM1/MOPAC implemented in DISCOVER/INSIGHT v.98). In the minimization a homogeneous electronic density was obtained for the hydrophobic backbone of the octamer molecule with a diameter of ~0.6 nm with only the histidine side chain protruding from it.

Further characterization of the aggregates on a solid surface

To study the behavior of the amphipathic peptide on a system that mimics an interface (membrane/extracellular matrix) we carried out additional observations of structures of the $(VHLPPP)_r$ (where $r = 1$, 3, and 8) peptides on the highly oriented pyrolytic graphite surface by atomic force microscopy imaging and contact angle measurements.

Atomic force microscopy studies

The aggregation of the peptide octamer over the hydrophobic substrate highly oriented pyrolytic graphite from an aqueous solution shows that the surface was covered entirely by domains of ~1 μm^2 formed by fibrils that are arranged side by side on the defined surface (Kogan et al., 2001). The average width of the fibrils was calculated as 6 ± 1 nm ($n = 30$). In recent experiments imaged in air, single molecular structures have been observed on top of the fibril layer (Fig. 7). The averaged height of the structures is always 1.2 ± 0.2 nm ($n = 5$), corresponding to the diameter of a PPII helix, and the length is 15 nm after correction for the convolution (which is almost the length of the octamer). Two aligned molecules having double length (~30 nm) are also evident in Fig. 7.

Imaging of the graphite surface in different aqueous solutions of the peptide with concentrations ranging from 10^{-11} to 10^{-6} M (around CAC), was carried out using in situ atomic force microscopy in tapping mode. These conditions, which are more physiologically relevant than air, confirmed the presence of 6 ± 1 nm ($n = 10$) fibrils. Within this concentration range, 10^{-11} to 10^{-6} M we tried to follow the fibril growth in situ, but the time (3–5 min) elapsed between the preparation of the liquid cell and the setup for image acquisition is enough to fully cover the surface with fibrils. We attempted to minimize this delay by adding the peptide solution after cell preparation using a flow system, but still time (1 min) was not enough to monitor layer formation. On the top of the fibril layer, the spontaneous formation of discontinuous multilayers was also observed, and Fig. 8 shows an example at 10^{-8} M concentration. Thus, step heights of monolayers are able to be measured in these discontinuous multilayers, giving a value of 6 ± 2 nm ($n = 5$), which coincides with the measured width of the fibril.

At the concentration range 10^{-6} to 10^{-3} M the entire graphite surface was covered by the fibril layer, and also the presence of big multilayers over the fibrils was observed (Fig. 9).

To understand the role of molecule size in the registered structures by atomic force microscopy, peptides with a lower number of repeats $(VHLPPP)_r$ ($r = 1$ and 3) have been studied. The formation of fibrils of 6 ± 1 nm ($n = 10$) in width also occurs for peptides $(VHLPPP)_r$ (where $r = 1$ and 3) observed in liquid conditions (Fig. 10).

Macroscopic behavior of the peptide solution over the highly oriented pyrolytic graphite: contact angle measurements

The hydrophobic or hydrophilic character of the surface induced by the peptide deposited on highly oriented pyrolytic graphite was subsequently investigated by contact angle measurements. A 1-μl drop of either milli-Q

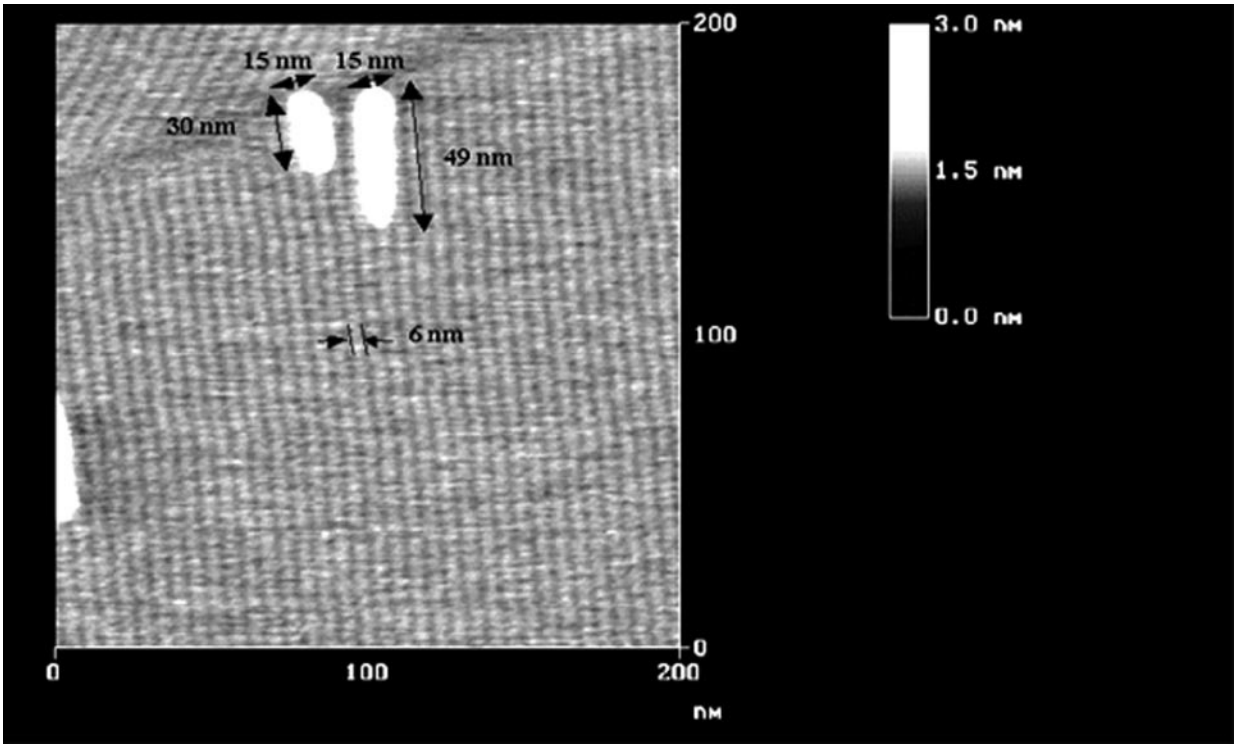

FIGURE 7 Tapping mode atomic force microscopy images in air of a sample prepared by fast drying of a 2×10^{-8} M aqueous solution of the peptide octamer $(VHLPPP)_8$ on a highly oriented pyrolytic graphite surface.

water or a 1×10^{-8} M solution of peptide were deposited on a freshly cleaved highly oriented pyrolytic graphite surface, and the contact angle was measured, being in both experiments $79 \pm 2°$ ($n = 5$). A 1-μl drop of milli-Q water deposited on top of a peptide layer, obtained after washing (without drying the surface) with water to remove the nonadsorbed peptide, also showed a contact angle of $79 \pm 2°$ ($n = 5$), confirming the hydrophobic character of the peptide layer. Atomic force microscopy observation of the same sample under a water drop con-

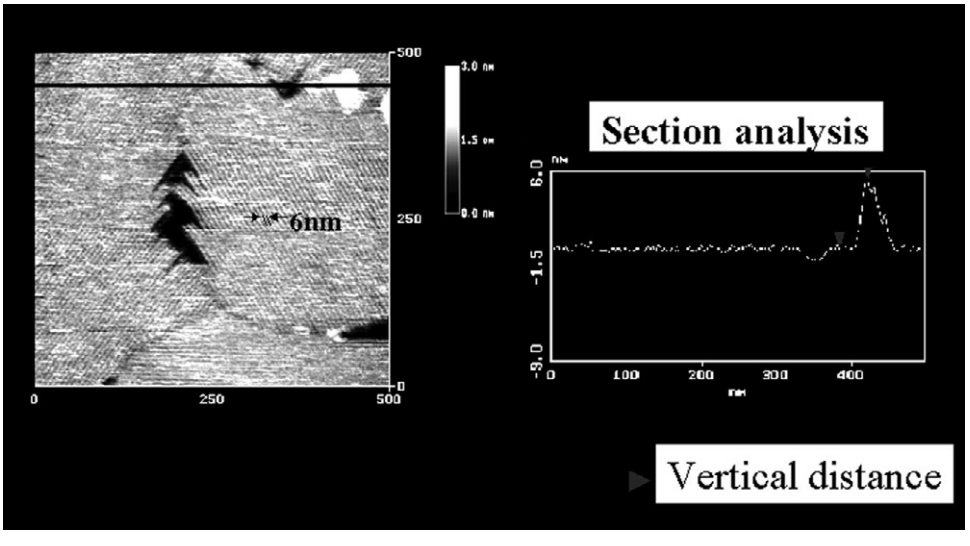

FIGURE 8 Tapping mode atomic force microscopy image in liquid of a 2×10^{-8} M aqueous solution of the peptide octamer $(VHLPPP)_8$ on a highly oriented pyrolytic graphite surface. The observed average width of the fibrils is 6 ± 1 nm. The formation of discontinuous multilayers can be observed with a measured step height of 5.8 nm.

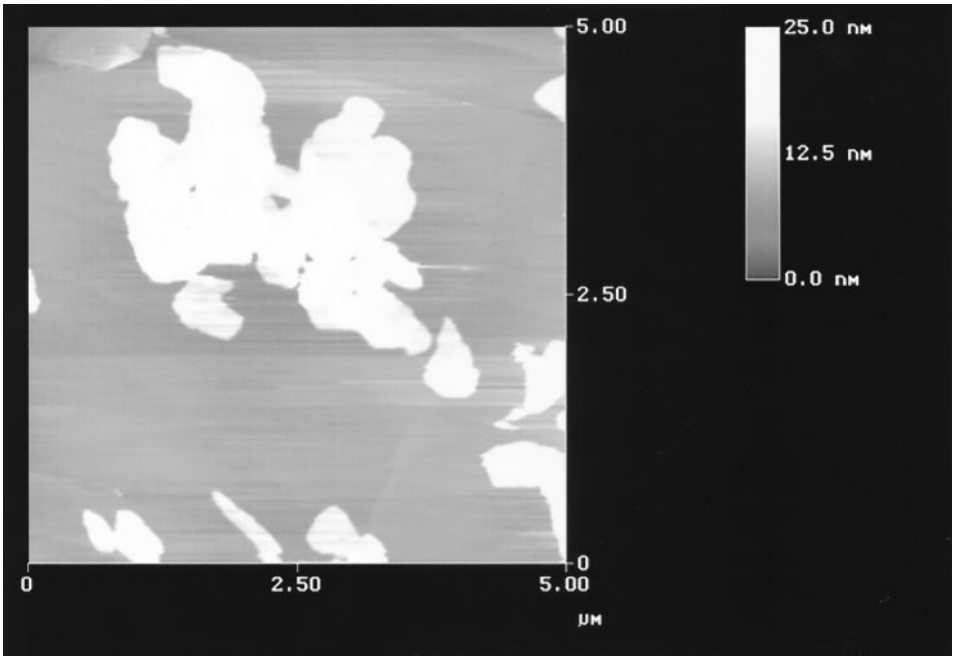

FIGURE 9 Tapping mode atomic force microscopy image in liquid of a 1×10^{-3} M aqueous solution of peptide $(VHLPPP)_8$ on a highly oriented pyrolytic graphite surface.

firmed the presence of a peptide layer formed by 6-nm-width fibrils (data not shown).

DISCUSSION

Physicochemical and spectroscopic characteristics of $(VHLPPP)_8$

The amphipathic nature of the $(VHLPPP)_8$ in its PPII conformation (Fig. 1) is demonstrated by the surface-active properties of the peptide. As can be seen in Fig. 2, $(VHLPPP)_8$ lowers the surface tension of water. The CMC of the octamer is 2×10^{-4} M (Fig. 2). However, the peptide $(VHLPPP)_8$ showed another critical concentration value of 4×10^{-7} M (the CAC) (Evans and Wennerström, 1999). At the concentration range above the CAC (4×10^{-7} to 1×10^{-4} M) the amphiphile can be separated at the surface and also forms micelles in the bulk. When the CMC is reached, the amphiphile species saturates the surface and aggregates in the bulk by micelle-association-forming superstructures. Similar behavior was also found in rod-shaped micelles

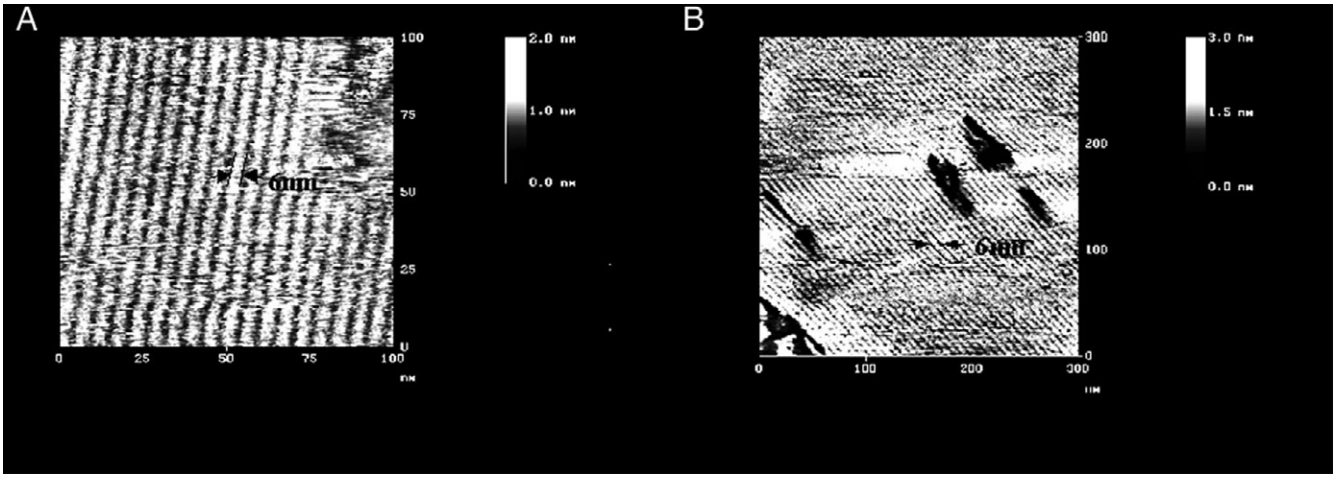

FIGURE 10 Tapping mode atomic force microscopy images in liquid of a 2×10^{-8} M aqueous solution of peptides $(VHLPPP)_r$ on a highly oriented pyrolytic graphite surface. The average width of the fibrils is 6 ± 1 nm. (*A*) $r = 1$; (*B*) $r = 3$.

FIGURE 11 Schematic view of cylindrical micelles from peptides $(VHLPPP)_r$ (where $r = 1$, 3, and 8). Molecules of peptides $(VHLPPP)_n$ in PPII conformation are represented by cylinders in which hydrophobic parts are shown in gray (i.e., the V and L residues) and hydrophilic parts in black (i.e., the H residues). The diagram summarizes a three-dimensional view of the longitudinal growth of a micelle, assuming a three-molecules lateral association. Notice the lateral interaction between the hydrophobic residues (gray part of molecules). The black parts remain exposed to the water. The longitudinal growth occurs by superposition of adjacently located molecules if the micelle is: $n = 1$ (*A*); $n = 3$ (*B*); and $n = 8$ (*C*).

formed by 3-alkylpolyglucosides (Balzer, 1991) and also for amphiphiles in the presence of polymers (Evans and Wennerström, 1999).

Circular dichroism experiments show a marked concentration dependence between the two critical concentrations. The maximum amphipathic character of $(VHLPPP)_8$ is displayed when it adopts the PPII conformation, and in this concentration range, micelle formation is apparently coupled to conformational transition from a disordered to a PPII conformation. Above 2×10^{-4} M, the CMC, the conformational equilibrium is completely shifted to the PPII conformation, so further changes in the surface activity, mentioned above, may be are related to the formation of superstructures or rearrangement of the existing micelles.

A micellar model for self-aggregation of $(VHLPPP)_8$ in aqueous solution agrees with small-angle x-ray scattering and transmission electron microscopy

The formation of cylindrical micelles can be explained by the self-assembling in aqueous solution of the amphipathic PPII helices of $(VHLPPP)_r$ peptides (where $r = 1$, 3, and 8). Fig. 11 shows a representation of the cylindrical micelles formed in aqueous solution where the cylinders represent the amphipathic $(VHLPPP)_r$ molecules, the hydrophobic faces (represented in gray containing the residues V and L) are hidden inside, and the polar faces (represented in black containing the H residues) are exposed to water. The longitudinal growth of the cylindrical micelles occurs by superposition of adjacently located molecules. The micellar model is compatible with the known dimensions of peptide molecule, but nothing is inferred from the inner structure of the micelles (i.e., the exact number of peptide molecules and the disposition of them into the cylindrical micelle).

The observation by transmission electron microscopy of a platinum replica of a freeze-fixed and freeze-dried peptide solution highlighted the presence of fibrillar superstructures with cylindrical filaments of 3 nm in width for all peptide concentrations (1×10^{-7} to 2×10^{-3} M). Moreover, the width of the filaments (3 nm), observed by transmission electron microscopy, is independent of the length of the peptide in the series $(VHLPPP)_r$ (where $r = 1$, 3, and 8). A similar cascade of aggregation events based on a rod-like molecular architecture has been observed for amphipathic synthetic polymers as polyphenylene ethylene derivatives (Schnablegger et al., 1999) and diblock phenylene vinylene ethylene glycol copolymers (Wang et al., 2000).

The CAC may be identified with the 3-nm-width filaments observed by transmission electron microscopy (cylindrical micelles), and the CMC may be related to the formation of the 20-nm superstructures also observed by transmission electron microscopy.

At 2×10^{-3} M (higher concentration than CMC), the size and the inner structures (3-nm-width filaments) corresponding to the fibrillar superstructure (20 nm) were confirmed by small-angle x-ray scattering. The model (Fig. 6) used for the simulation of the small-angle x-ray scattering measurements agrees with the transmission electron microscopy results. Thus, Fig. 6 depicted the superstructure of the peptide in aqueous solution.

Interaction of the γ-zein N-terminal domain with the interface graphite-water

A micellar model can explain the fibril formation of the different peptides $(VHLPPP)_r$ (where $r = 1$, 3, and 8) on the hydrophobic highly oriented pyrolytic graphite surface. The surface is initially covered by single molecules of peptides $(VHLPPP)_n$ exposing their hydrophobic side (V and L residues, represented in the gray part of the cylinder) to the substrate and leaving their hydrophilic side (H residues, represented in the black part of the cylinder) facing the water (Fig. 12 *A*). To know the plausibility of this extreme, we carried out a molecular dynamics simulation during 500 ps at 300 K using a continuum media with a dielectric constant $\epsilon = 70$ and consistent valence force field (implemented in DISCOVER/INSIGHT II v.98) as a force field. Three molecules of the peptide were put parallel with each other over a graphite surface, so that the peptide molecules remained self-assembled and adsorbed to the graphite surface with the hydrophobic parts of the molecule interacting with graphite and the hydrophilic part exposed to the media (data not shown). Over the surface covered with peptide molecules, the cylindrical micelle may then be segregated from the bulk over this surface (Fig. 12 *A*) and alternatively

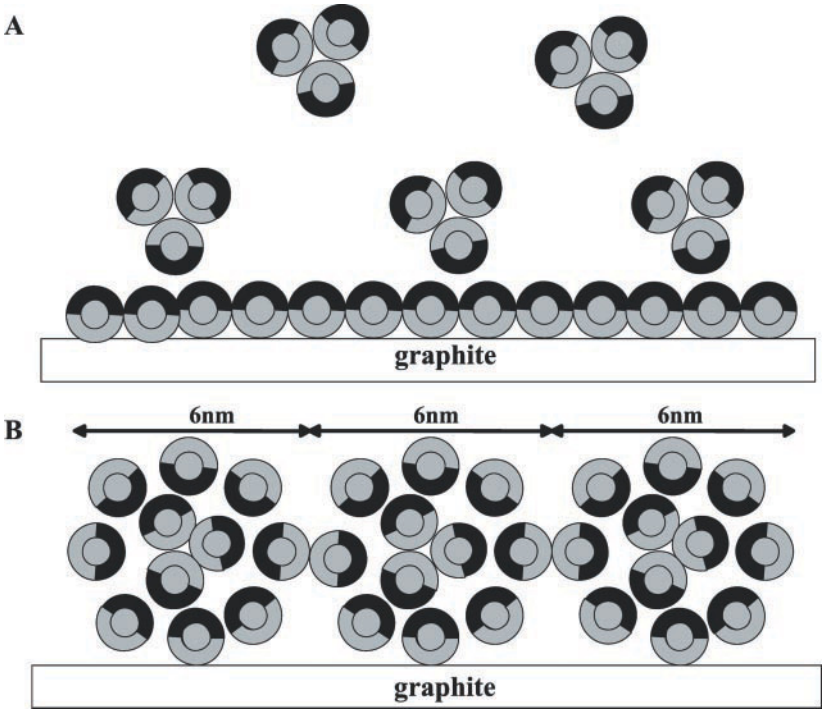

FIGURE 12 Schematic representation of fibril formation. (*A*) highly oriented pyrolytic graphite surface (gray) coated by peptide molecules (black and gray cylinders). Hydrophobic parts (in gray, corresponding to V and L residues) interact with the highly oriented pyrolytic graphite surface, whereas hydrophilic parts (in black, corresponding to the H residues) remain exposed to the water. The aqueous peptide micelle (here represented by three molecules of peptide) is placed over this coated surface; thus, the polar zones of the aqueous peptide micelle come in contact with the polar zones of the peptide deposited over the surface. Other micelles are in the bulk. (*B*) Schematic view of the aqueous micelles coated by molecules of the peptide deposited (fibrils) over the highly oriented pyrolytic graphite surface. The modeled diameter of the fibril is 6 nm. Frontal view of the fibrils assembled on the graphite substrate with a 6-nm periodicity.

may associate to form superstructures of 20 nm. In the concentration range below the CMC, the formation of 20-nm superstructures will have a low probability, and the expected mechanism is segregation of the amphiphile on the surface of the cylindrical micelles. In Fig. 12 *B*, the cylindrical micelle has been surrounded by other peptide molecules that help to form the 6-nm fibril. The hydrophobic lateral interaction between the fibrils determines their parallel orientation on highly oriented pyrolytic graphite and the formation of the stable hydrophobic coating that is not washed easily by water and that gives a contact angle with water similar to that of graphite. In the transient from Fig. 12 *A* to Fig. 12 *B* the incorporation of peptide molecules can be done as isolated molecules or as cylindrical micelles because in solution a micellar dissociation equilibrium exists. From the analysis of fibril images both in air and in situ liquid we conclude that graphite does not induce orientation of the peptide molecules; that is, the molecular rotation is free on the plane of the surface. Fibril domains with arbitrary orientation have been imaged on an isolated graphite terrace. Two-dimensional structures (the multilayers) have been also observed over the original graphite fibrils mainly for higher concentrations than CMC. We conclude that atomically flat graphite surface has the ability to dispose molecules to form the fibrils, which is not the case of the surface offered to solution by the monolayer of these two-dimensional crystallized fibrils.

The width of the fibrils observed by atomic force microscopy is independent of the length of the peptide in the series $(VHLPPP)_r$ (where $r = 1$, 3, and 8). This is in agreement with the similar observations made by transmission electron microscopy in solution and confirms that individual molecules are aligned with their long dimension in the direction of the fibrils. This is also compatible with the individual molecules oriented along the fibril axis. These results have led us to reject our first geometric model in which the fibril width depends on the peptide length (Kogan et al., 2001) and lend support to a micellar model.

The ability of the peptide $(VHLPPP)_8$ to form fibrils is in agreement with the suggestion made by Lending (1996) in which zeins (other than the α-zein) could also form tubular arrays at the rough ER of opaque-2 maize. We cannot discard that peptides containing a smaller number of repeats could form tubular arrays. We found that peptides $(VHLPPP)_r$ where ($r = 1$ and 3) have the ability to form cylindrical aggregates. In fact in maize protein bodies, γ-zein-like proteins with shorter repetitive domains comprising only two complete hexapeptides and two truncated hexapeptides of five and three residues, respectively, exist (Shewry and Tatham, 1990).

The self-assembly of the amphipathic peptide in aqueous solution and the behavior of the octamer in the highly oriented pyrolytic graphite/water interface suggest a role of the N-terminal domain of γ-zein in the formation of protein bodies. The amphipathic structure and the ability of γ-ZNPRD to self-assemble may induce a coat in the inner face of the ER membrane. This coating may then be covalently stabilized via intramolecular disulfide cross-linking involving either the cysteine-rich γ-zein C-terminal domain or the cysteine residues flanking the γ-ZNPRD. Experiments us-

ing lipid bilayers and γ-zein are currently in progress to validate this model.

We thank Dr. Dolors Ludevid for fruitful discussions. We thank Francisco Comelles for assistance with surface tension measurements at the Departamento de Tecnologia de Tensioactivos (Instituto de Investigaciones Químicas y Ambientales de Barcelona, CSIC). We thank David Bellido for assistance with transmission electronic microscopy experiments at Serveis Científico-tècnics of the Universitat de Barcelona. We thank to Marisol Cuñaro for assistance with measurements of drop contact angles at Serveis Científico-tècnics of the Universitat de Barcelona.

This work has been supported by a fund from CICYT (B1099–0484) and Generalitat de Catalunya (CeRBa and Grup Consolitat). M.J.K. is grateful to CONICET (Argentina) for a postdoctoral fellowship.

REFERENCES

Balzer, D. 1991. Alkylpolyglucosides, their physicochemical properties and their uses. *Tenside Surfactants Deterg.* 28:419–427.

Blanch, E. W., A. Morozova-Roche Ludmilla, A. Duncan, E. Cochran, A. J. Doig, L. Hetch, and L. D. Barron. 2000. Is polyproline II helix the killer conformation? A Raman optical activity study of the amyloidogenic prefibrillar intermediate of human lysozime. *J Mol. Biol.* 301: 553–563.

Dalcol, I., M. Pons, M. D. Ludevid, and E. Giralt. 1996. Convergent solid phase of repeating peptides (Val-X-Leu-Pro-Pro-Pro)$_8$ adopting a polyproline II conformation. *J. Org. Chem.* 61:6775–6792.

Dalcol, I., F. Rabanal, M. D. Ludevid, F. Albericio, and E. Giralt. 1995. Convergent solid phase peptide synthesis: an efficient approach to the synthesis of highly repetitive protein domains. *J. Org. Chem.* 60: 7575–7581.

Evans, F. D., and H. Wennerström. 1999. The Colloidal Domain Where Physics, Chemistry, Biology and Technology Meet. Wiley-VCH, New York.

Geli, M. L., M. Torrent, and M. D. Ludevid. 1994. Two structural domains mediate two sequential events in gamma zein targeting: protein endoplasmic reticulum retention and protein body formation. *Plant Cell.* 6:1911–1192.

Gill, A. C., M. A. Ritchie, L. G. Hunt, S. E. Steane, K. Davies, S. P. Bocking, A. G. O. Rhie, A. D. Bennett, and J. Hope. 2000. Post-translational hydroxylation at the N-terminus of the prion protein reveals presence of PPII structure in vivo. *EMBO J.* 19:5324–5331.

Galtter, O. 1990. Neutron, X-Ray and Light Scattering, Vol 33. P. Lindner and T. Zemb, editors. North Holland, Amsterdam.

Herman, E. M., and B. A. Larkins. 1999. Protein storages bodies and vacuoles. *Plant Cell.* 11:601–613.

Kogan, M. J., I. Dalcol, P. Gorostiza, C. Lopez-Iglesias, M. Pons, F. Sanz, M. D. Ludevid, and E. Giralt. 2001. Self-assembly of the amphipathic helix (VHLPPP)$_8$: a mechanism for zein protein body formation. *J. Mol. Biol.* 312:907–913.

Lending, C. R. 1996. A novel tubular array associated with protein bodies in the rough endoplasmic reticulum of *opaque*-2 maize. *Protoplasma.* 195:68–77.

Lloyd-Williams, P., F. Albericio, and E. Giralt. 1997. Chemical Approaches to the Synthesis of Peptides and Proteins. CRC Press, Boca Raton, FL.

Ludevid, M. D., M. Torrent, J. A. Martinez-Izquierdo, P. Puigdomenech, and J. Palau. 1984. Subcellular localization of glutelin-2 in maize (*Zea Mays L.*) endosperm. *Plant Mol. Biol.* 3:227–234.

Newman, A. W., and R. J. Good. 1979. Techniques of Measuring Contact Angles. *In* Surface and Colloid Sciences: Experimental Methods. R. J. Good and R. R. Stromberg, editors. Plenum Press, New York. 33–37.

Pedersen, J. S. 1997. Analysis of small-angle scattering data from colloids and polymer solutions: modelling and least-squares fitting. *Adv. Colloid Interface Sci.* 70:171–210.

Porod, G. 1982. General theory. Small-Angle X-Ray Scattering. O. Glatter and O. Kratky, editors. Academic Press, New York. 17–51.

Rabanal, F. M., Ludevid, D., Pons, M., and E. Giralt. 1993. Circular dichroism of proline-rich polypeptides: application to study of the repetitive domain of maize glutelin-2. *Biopolymers.* 33:1019–1028.

Schnablegger, H., M. Antonietti, C. Göltner, J. Hartmann, H. Cölfen, P. Samori, J. P. Rabe, H. Häger, and W. Heitz. 1999. Morphological characterization of the molecular superstructure of polyphenylene ethynylene derivatives. *J. Colloid Interface Sci.* 212:24–32.

Shewry, P. R., and A. S. Tatham. 1990. The prolamin storage proteins of cereal seeds: structure and evolution. *Biochem. J.* 267:1–12.

Showalter, A. M. 1993. Structure and function of plant cell wall proteins. *Plant Cell.* 5:9–23.

Singh, M. A., S. S. Ghosh, and R. F. Shannom. 1993. A direct method of beam-height correction in small-angle x-ray scattering. *J. Appl. Crystallogr.* 26:787–794.

Staub, O., and D. Rotin. 1996. WW domains. *Structure.* 4:495–499.

Stern, L. J., J. H. Brown, T. S. Jardesky, J. C. Gorfa, R. G. Urban, J. L. Stroninger, and D. C. Wiley. 1994. Crystal structure of the human class II MHC protein HLA-DR1 complexed with an influenza virus peptide. *Nature.* 368:215:221.

Wang, H., H. H. Wang, V. S. Urban, K. C. Littrell, P. Thiyagarajan, and L. Yu. 2000. Synthesis of amphiphilic diblock copolymers containing a conjugated block and their self-assembling properties. *J. Am. Chem. Soc.* 122:6855–6821.

Williamson, M. 1994. The structure and function of proline-rich regions in proteins. *Biochem. J.* 297:249–260.

Wu, X., B. Knudsen, S. M. Feller, J. Zheng, A. Sali, D. Cowburn, H. Hanafusa, and J. Kuiryan. 1995. Structural basis for the specific interaction of lysine-containing proline-rich peptides with the N-terminal SH3 domain of c-Crk. *Structure.* 3:215–226.

Zemb, T. N., S. T. Hyde, P-J. Derian, I. S. Barnes, and B. W. Ninham. 1987. Microstructure from x-ray scattering: the disordered open connected model of microemulsions. *J. Phys. Chem.* 91:3814–3820.